A statistical study of Galactic SNR source spectra detected at >GeV energies

Matthias Mandelartz and Julia Becker Tjus

Ruhr-Universität Bochum, Fakultät für Physik & Astronomie, Theoretische Physik I, D-44780 Bochum, Germany

matthias.mandelartz@rub.de

Abstract

Broadband modeling of 24 Galactic supernova remnants was performed using a model to test the SNRs for hadronically generated γ-rays by examining combined spectra of π^0-decay, bremsstrahlung, inverse Compton, and synchrotron radiation. After now more than 7 years of data taking with H.E.S.S., MAGIC, and VERITAS and after more than 4 years with Fermi in operation, a full broadband data set of 24 Galactic SNRs exists. This is the first statistical study of the resulting source spectra, which are reviewed individually to ascertain the origin of the gamma radiation. This allows a combined examination to test the current prepositions of particle acceleration.

1. Introduction

Supernova remnants (SNRs) are commonly believed to be responsible for a major contribution to the cosmic rays (CR) measured at Earth, as they can accelerate particles up to PeV energies (Hillas 2005) via diffusive shock acceleration (Blandford and Ostriker 1978). Although SNRs have been studied for years there has been no agreement on whether the γ-rays emitted by them are of leptonic or hadronic origin.

Supernova remnants are usually studied — concerning their γ-ray emission — by modeling a specific emission process in a specific geometry. For the emission of SNRs interacting with molecular clouds there have been extensive studies from various people ranging from a diffusive approach (Li and Chen 2012) to the prediction of ionization signatures induced by protons if the emission is of hadronic nature (Becker et al. 2011; Schuppan et al. 2012). Leptonic models usually use precomputed spectra originating from approximatively solved differential equations, like Zirakashvili and Aharonian (2007). Preselecting the emission scenario can be dangerous, as certain types of emission dominate over others in a (n_H, B)-space, which can be seen in Figure 1.

In this paper a simple model is used for fitting the broadband emission of Galactic SNRs by minimizing χ^2 to determine the origin of the gamma radiation emitted by the SNRs, while not focusing on a particular scenario. The total energy in magnetic field and CRs is used to disqualify certain emission scenarios as realized if the non-thermal energy threshold for SNRs ($\sim 10^{52}$ ergs) is exceeded. The commonly used assumptions in Beck and Krause (2005) for calculating the magnetic

field strength where the total energy is at its minimum — as this is the scenario which is most likely to be realized at the sources — do not hold in this study as neither the number of accelerated protons and electrons nor their power-law indices do match. Nevertheless the minimization of total energy is used as a criterion to ascertain the scenario which is most likely realized at the source.

2. Modeling

The model used in this work assumes that the prevalent particle spectrum at the source can be described by a power-law in the momentum of the particles (Schlickeiser 2002). The spectrum exhibits the features of a maximum energy E_{max} and a minimum energy E_{min}. The cut-off for the maximum energy is induced by an exponential function and the cut-off behavior for the minimum energy is induced by a hyperbolic-tangent function. After transforming the momentum spectrum to an energy spectrum, the primary spectrum $j_X(E)$ for a particle species X can be described by the following function

$$j_X(E) = a_X \left(\frac{\sqrt{E^2 + 2Em_Xc^2}}{\sqrt{E_0^2 + 2E_0m_Xc^2}} \right)^{-\alpha_X} \frac{E + m_Xc^2}{\sqrt{E^2 + 2Em_Xc^2}} \tanh\left(\frac{E}{E_{\mathrm{min},X}} \right) \exp\left(-\frac{E}{E_{\mathrm{max},X}} \right). \quad (1)$$

Here, a_X is a normalization constant of the dimensions per energy per volume and α_X the power-law index.

The maximum energy E_{max} for protons was chosen to be 1 PeV, in case of electrons the cut-off energy could be fitted due to the X-Ray emission of the remnants. If no X-Ray data were prevalent, a suitable cut-off roughly consistent with the observations has been chosen.

The maximum energy is usually believed to be caused as an acceleration limit or by synchrotron cooling, which both cases depend on the shock speed. As the shock speed decreases with the age of the remnant, a decline in the maximum energy depending on the remnant can be expected.

The minimum energy was chosen to be 10 MeV for the protons in accordance with Padovani et al. (2009), and in case of the electrons 0.511 MeV was used, when more detailed observations were unavailable.

Based on the particle spectrum at the source, emitted photons can be expected from the interactions with surrounding matter. Various processes have been taken into account: The emission of primary electrons was modeled as synchrotron, bremsstrahlung and inverse Compton spectra in accordance with the work of Blumenthal and Gould (1970). The inverse Compton radiation was calculated for scattering on the CMB only, while bremsstrahlung was emitted of electrons due to the interaction with molecular and atomic hydrogen and helium. For the helium to hydrogen ratio, the standard ISM ratio was assumed and the emission was modeled according to Schlickeiser (2002).

The gamma radiation emitted by the primary proton spectrum was modeled via proton-proton-interactions (Kelner et al. 2006) from the spectrum with the ambient gas.

The resulting photon spectra out of these interactions were fitted in a predetermined way to the observed radiation flux of the remnant by minimizing the χ^2. The minimization was performed using the Nelder-Mead algorithm (Nelder and Mead 1965) as implemented in the GSL (Galassi

et al. 2009).
The fitting process was split into two seperate fits: One for the electron spectrum and one for the proton spectrum. In the first step, it was assumed that the entire emission from the remnant was dominated by the radiation emitted by electrons, so that with a fixed gas density the magnetic field strength had to be another fitting parameter in addition to the parameters that are necessary due to the spectral shape of the assumed particle spectrum. The magnetic field strength determined that way serves as the infimum of the magnetic field strength in the the computation.
In a second step the assumption of the completely electron-dominated spectrum was dropped. The magnetic field strength was increased stepwise and the electron spectrum was fitted to the observed synchrotron radiation. Due to a lower magnetic field strength, less electrons were needed to emit the observed synchrotron radiation, which leads to a decrease of γ-rays emitted due to bremsstrahlung and IC-radiation. This gap was filled by fitting additionally the π^0-decay emission by protons to the spectrum to match the observed gamma radiation again to the emitted radiation. This way a profile of each remnants emission depending on the magnetic field strength was obtained.
It was assumed that the combined energies of the primary electron and proton spectra and the magnetic field should be at a minimum, given that the theoretical SED explains the observed electromagnetic emission by the remnant.

3. Results

It is shown via the semianalytical approach by Kelner et al. (2006) for the calculation of the π-decay spectra, the non-thermal emission from secondary electrons and positrons can be neglected. The calculated flux ratio of primary protons to secondary electrons and positrons is displayed in Figure 2. It can be expected that non-thermal emission can be neglected anywhere in the Milky Way.
When discussing the results in the following two scenarios are distinguished:

Hadronic Scenario This refers to a hadronically dominated γ-ray SED, given that the said SED does not need much more energy than the purely leptonic case or a hybrid scenario.

Minimum Energy Scenario The minumum energy scenario refers to the theoretical SED configuration that explains the observed SED well, and minimizes the total non-thermal energy.

3.1. Individual SNRs

In this subsection, a short discription of the modeling of the individual remnants is given. The best fit scenario for the minimum energy case is shown in Figure 3 and 4. Figure 5 and 6 shows the total non-thermal energy budget for the different magnetic field configurations. A summary of the behavior of the specific remnants is displayed in Table 1. All references used for the modeling

of the remnants are given in Table 2.

3.1.1. W28

This subsection deals with the HESS J1801–233 TeV γ-ray source. A hybrid model seems to be the most favored one for this supernova remnant, explaining the GeV γ-ray emission (Abdo et al. 2010b) by gamma radiation produced by π^0-decay and the TeV γ-ray emission (Aharonian et al. 2008d) by bremsstrahlung from electrons that are responsible for the synchrotron emission, too.
A case where the gamma radiation is completely generated by protons is unlikely, as the magnetic field strengths required to suppress the bremsstrahlung would exceed energies of 10^{52} ergs in the magnetic field.

3.1.2. W28C

G5.7–0.1, also referred to as W28C, is a supernova remnant that was discovered not too long ago (Brogan et al. 2006). There are still doubts that it actually is a supernova remnant because of its irregular morphology, which lead Brogan et al. (2006) to a classification of the object as a class III supernova remnant. Apart from the measurements by H.E.S.S. (Aharonian et al. 2008d) there exists a number of upper limits from Fermi-LAT (Abdo et al. 2010b). The observed spectrum leads to the conclusion that the high-energy part of the spectrum is probably generated by bremsstrahlung emission, although it is not entirely certain. There is still a high probability that the observed gamma radiation is of hadronic origin.

3.1.3. W30

The modeling of W30 faces one central difficulty, namely the upper limit imposed by Fermi-LAT. A single zone radiation model always fails to explain the observed radiation, as a triple broken power-law would be needed to explain the γ-radiation. While Ajello et al. (2012) use a two-zone hadronic model to explain the SED, the simple power-law approach suggests that the H.E.S.S. data can be explained by a combination of bremsstrahlung and IC-radiation and the radiation measured by Fermi-LAT is of hadronic origin. This scenario needs less energy than a two-zone model for the remnant.

3.1.4. W33

The modeling of supernova remnant G12.8–0.0 favors a leptonic model, which confirms Albert et al. (2006a), although it is not certain with flux measurements in the H.E.S.S. energy range only.

A hadronic component could not be identified as the fit would have indicated power-law spectra with an index of ~ 1.0 for scenarios that needed slightly more of energy more than purely leptonic models.

3.1.5. W41

The supernova remnant G23.3–0.3 is one of the rare cases for which every scenario is possible: A purely hadronic scenario, a mixed model and a leptonic model. The minimum energy argument implies that the emission is of leptonic origin contrary to the assumptions of Li and Chen (2012), as a mixed model or a hadronic one requires up to two orders of magnitude more energy to sustain this radiation with the proton density of $6\,\mathrm{cm}^{-3}$ suggested by Leahy and Tian (2008).

3.1.6. 3C391

The nature of the modeled SNR 3C391 was determined to be hadronic — which confirms the assumptions of Castro and Slane (2010) — although an electron spectrum flattened by bremsstrahlung might work equally well. This scenario was dismissed as such an electron spectrum is difficult to reproduce within the used framework.

3.1.7. W44

The different modeled SEDs of the supernova remnant G34.7–0.4 show only one unique match for the observed radiation. The gamma radiation observed by Fermi-LAT and AGILE is of hadronic origin, while dominating a flat bremsstrahlung spectrum with an photon index of about ~ 2.0. Uchiyama et al. (2012). This confirms the hadronic modeling by Uchiyama et al. (2012). Yet unclear is the exact shape of the electron spectrum, a more detailed analysis has to be performed for W44 to determine the leptonic part of the radiation more precisely.

3.1.8. G40.5–0.5

The electron spectrum of G40.5–0.5 is supposed to cut off at energies lower than the measured radiation. So the measured radiation from G40.5–0.5 is unambiguously of hadronic origin. Due to the high gamma flux of the remnant it is one of the primary candidates for the detection of neutrino emission from Galactic SNRs, see section 3.3.

3.1.9. W49B

The SNR W49B has a very steep photon spectrum, while the electron spectrum to explain the synchrotron radiation is rather soft. The gamma photon spectral index is at least 0.5 higher than the electron power-law index. This means that the gamma radiation must originate from hadronic processes, which confirms Abdo et al. (2010e). An influence of the electrons might be present at higher energies before they cut off.

3.1.10. W51C

The remnant W51C was challenging to model with a simple power-law behavior. The major difficulty arises from the size of the remnant. Even with the suggested density of $n_{\mathrm{H}} = 10\,\mathrm{cm}^{-3}$ by MAGIC (Aleksić et al. 2012) it was difficult to stay below the total threshold energy of $10^{52}\,\mathrm{ergs}$, as the minimum magnetic field energy was estimated to be $E_{B_{\mathrm{min}}} = 1.3 \times 10^{51}\,\mathrm{ergs}$. Nevertheless, the modeling confirms Aleksić et al. (2012) with a hadronic model. Although the fluxes measured by H.E.S.S. are likely to be heavily influenced by bremsstrahlung emission.
Although a two-zone leptonic model is also possible, and needed if the density is at least 5 times as large. In case of such a model one zone could be responsible for the γ-ray emission via bremsstrahlung emission, and the other zone would be responsible for the synchrotron emission.

3.1.11. Cygnus Loop

The complete Cygnus Loop SED might be explained by an electron spectrum that exhibits a bremsstrahlung-flattened synchrotron peak. As there were no data indicating that this is realized, this scenario is not considered further here. A spectral index of ~ 2.0 for the electron spectrum based on the radio measurements was found from the fit. This does not match the gamma photon index, so that the gamma radiation has to be of hadronic origin, which was also concluded by Katagiri et al. (2011).

3.1.12. Cas A

The bump in Cas A's SED around 10 GeV could be explained by a high lower cut-off energy in the same order of magnitude in the electron spectrum so that bremsstrahlung is responsible for the observed gamma radiation, but the synchrotron radiation does not cut off at these energies. So this scenario is dismissed while a hadronic scenario was pursued, which explains the observed fluxes except for the second upper limit well.
In case of a bremsstrahlung-dominated Fermi energy-range in the SED, hadronic interactions would still be responsible for a major part of the spectrum as the IC radiation from the electrons would

fail to explain the TeV data completely.

3.1.13. Tycho

Tycho's SNR is one of the prime examples when it comes to hadronically generated gamma radiation (Giordano et al. 2012; Morlino and Caprioli 2012). This work also confirms this, given that the density used by various calculations is close to the actual value. As the electron and proton power-law indices have — within errors — the same value the gamma radiation could be reproduced at a high density $n_{\mathrm{H}} > 50\,\mathrm{cm}^{-3}$ by bremsstrahlung instead of proton-proton interactions.

3.1.14. IC443

IC443 was interesting, as it is usually modeled by hadronic interactions (Abdo et al. 2010d; Li and Chen 2012), but suppressing the leptonic gamma radiation completely requires magnetic field strengths that are up to 5 times larger, than the magnetic fields of the minimum energy scenario. This means that the majority of the γ-ray emission is of leptonic origin with an underlying hadronic component that rises at higher energies above the leptonic part explaining the Milagro data. The unusual cut-off from the plateau, which is not as steep as normal exponential cut-off can also be explained by this scenario.

3.1.15. Puppis A

From an energy minimizing persepective the SED of the SNR Puppis A is dominated by leptonic synchrotron and bremsstrahlung emission. While π^0-decay might play a major role for higher energetic gamma radiation, the data from Fermi-LAT is most likely dominated by leptonic emission. Additional measurements have to be performed to confirm this scenario as solely the data of Fermi-LAT is not sufficient to determine the origin of the radiation and the proton spectrum.

3.1.16. Vela Jr

Vela Jr has a similar SED as RX J1713.7–3946. A hadronic case would need an order of magnitude more energy than solely leptonic emission (see also Tanaka et al. 2011) which could explain the SED well and still requires only minor corrections, which could be due to hadronic emission. This would imply that another component in the SED might be visible at energies higher than the H.E.S.S. measurements, which would help in determining the proton source spectrum accurately.

3.1.17. MSH 11–62

MSH 11–62 has recently been found in γ-rays by Slane et al. (2012). Due to the lack of data for the SED of the remnant — without Fermi's upper limits, there were only 8 data points in total — the modeling carries large uncertainties. The radiation would need less energy if produced by protons compared to an electron generated SED; although both electron and proton mean power-law indices are significantly below the value of 2.0, their errors reach up to these values. With such large errors, it is not certain that the spectrum follows a power-law distribution.

3.1.18. RCW 86

As hadronic models without cut-offs fail to explain the upper limit in the SED measured by H.E.S.S. they can be excluded, as the leptonic spectrum that is responsible for the synchrotron radiation can already account for a cut-off in the spectrum in the needed energy range. It can be concluded that the radiation measured by H.E.S.S. is IC radiation if protons are assumed to reach up to the cosmic ray knee at PeV energies. Lemoine-Goumard et al. (2012) also note the difficulties explaining the radiation by hadronic processes. If protons are accelerated at this remnant the presence of hadronic gamma radiation still has to be confirmed at this specific SNR.

3.1.19. SN1006

The SED of the remnant SN1006 is missing measurements in the Fermi-LAT energy range, although the data by H.E.S.S. (Acero et al. 2010) agree well with a power-law with an index of ~ 2.35. Nevertheless it is very likely that the γ-ray emission measured by H.E.S.S. is indeed mainly produced by IC radiation. While a hadronically-dominated SED in the H.E.S.S. energy range would only require up to one magnitude of energy more than its current state or with a small hadronic contribution to the flux, it is unlikely as the source is not present in the latest source catalog of the Fermi-LAT collaboration (Nolan et al. 2012), implying rather strong limits and thus cut-off towards lower energies.

3.1.20. RX J1713.7–3946

The spectral shape of RX J1713.7–3946 is subject to debate, as the absence of line emission in the keV energies is taken as a hint that electrons are responsible for the gamma radiation, which does not have to be the case (Inoue et al. 2012). The data agrees well with an IC-dominated SED, but partially fails to account for the Fermi-LAT data. This strongly suggests that either bremsstrahlung or π^0-decay is more dominant in that energy range. Due to the low density usually used for modeling RX J1713.7–3946, a π^0-decay component is far more likely, but a π^0-decay-dominated spectrum can

be excluded, as the energy required for it is two magnitudes larger than the IC-dominated scenario.

3.1.21. CTB37A

The purely leptonically dominated model fails to account for the measured gamma radiation in the GeV energy domain, thus the SED is dominated by π^0-decay. A field strength of up to $B \sim 100\,\mu$G has to be expected for this case. From the point of energy minimization, a two-zone leptonic model should work better than hadronic emission, but as it requires a more complex geometry a clear favorite cannot be made out.

3.1.22. CTB37B

The hadronic scenario is steep enough to be seen by Fermi-LAT at lower energies, so that the absence from the source catalog (Nolan et al. 2012) can only mean that the spectrum flattens towards lower energies. This implies that the radiation measured by the H.E.S.S. telescopes to be of leptonic origin. However, a hadronic component with a power-law index of ~ 2 might be present with a lower flux than the IC-peak measured by H.E.S.S.

3.1.23. G349.7+0.2

A solely leptonically generated SED fails to explain the peak fluxes of the Fermi-LAT data, so that the γ-rays measured by Fermi-LAT are, with a high probability, of hadronic origin, which was assumed by Castro and Slane (2010). In this case, however, the flux of the first data point from Fermi-LAT is overestimated, which might be lower due to diffusive and other losses.

3.1.24. G359.1–0.5

Three of the Fermi-LAT data points cannot be matched unless the spectrum is dominated by bremsstrahlung in this domain, so this SED does not leave much room for interpretation. Additionally one might consider the energy minimization scenario, which indicates that a hadronically dominated SED requires energies of at least 10^{52} ergs, which is two orders of magnitude higher than in the leptonically dominated scenario.

3.2. Spectral Behavior

As a large amount of modeled supernova remnants have an error on their electron or proton power-law index that is of the order of 0.1–0.2, the bin size for histrograms concerning the distribution of spectral indices was chosen to be 0.2 to maintain a basic comparability between the electron power-law index histogram and the proton power-law index histogram. The electron power-law index is expected to peak around values of 2 for strong shocks (Bell 1978). The distribution does scatter around 2. Values much smaller than 2 might have been caused by a non-ideal treatment of the electron spectrum and missing out a proper calculation of free-free absorption.
Overall a good agreement with theory is found for the electron power-law index. The graph for the distribution of the hadronic power-law index, displayed in Figure 8, does not show the same distribution as the electrons. In that histogram both the hadronic and the equipartition scenario are shown, and the actual distribution can be expected to be somewhere between the two scenarios. The distribution peaks for power-law indices $2.1 < \alpha_p < 2.3$. There seems to be a second peak for power-law indices of $\alpha_p \gtrsim 2.6$. This does not seem to be due to a systematic or statistical error, but hinting that another concept has to underly those supernova remnants. It can thus be differentiated between two kinds of hadronically dominated supernova remnants from their γ-ray spectrum:

Class I A power-law index of $2.0 < \alpha_p < 2.3$. This class is from its current spectral energy distribution in the MeV–TeV domain indistinguishable from the shape of a bremsstrahlung dominated spectrum.

Class II A power-law index of $\alpha_p \gtrsim 2.6$. A sharp hadronic peak with a sudden decline exists in the MeV–GeV domain. The GeV–TeV domain is commonly dominated by bremsstrahlung or inverse Compton radiation in those cases.

The existance of those two classes still has to be confirmed by more statistics. These classes reveal different properties concerning their modeling: For Class I it is common that the γ-rays produced through π^0-decay are not dominant in the MeV–GeV range in this case, but rather photons produced by bremsstrahlung. This means that the hadronic origin of the MeV–TeV spectrum can only be confirmed by TeV measurements, at energies higher than the cut-off energy in the spectral energy distribution that is induced by electrons.
It is not clear whether the power-law index of the spectrum of Class II supernova remnants is really that steep or if the spectrum follows some other kind of distribution. The observed spectrum cannot be attributed to aging effects, as the remnants in this category are young, middle aged and old remnants, which can be seen comparing Table 1 and Table 2. It should be noted, however, that this classification still needs to be confirmed by higher statistics.
In Figure 9 the proton spectral index is plotted against the electron spectral index. The spectral indices obtained through modeling the supernova remnants with their respective errors are recorded in the graphic. Empirical data in nature rarely follow power-laws with an index smaller than 2 (Clauset et al. 2009), so that the region with an index smaller than 1.85 was considered as unphysical parameter space, crossed out in gray in the graph; but all modeled supernova remnants

are compatible with physics considering their 1σ error bars. Most of the power-law indices of the proton spectrum are larger than the power-law indices of the electron spectrum. This effect does seem to reflect the presence of Class II supernova remnants, as only two data points are below the line with the slope of 1.
In Figure 10, the cut-off energies are plotted against the ages of the supernova remnants. Only cut-off energies implied through X-Ray observations were used in that graph. The decline is evident. This was expected as the maximum energy reachable is linked to the shock speed of the remnant, which in turn decreases with the remnants age (Cox 1972).

The modeling raises the question of the nature of the higher proton power-law index compared to the electron power-law index, as shown in Figure 9. There are various explanations ranging from diffusion (Aharonian and Atoyan 1996; Strong et al. 2007) to deteriorated particle confinement (Malkov et al. 2012). There are various suggested mechanisms that lead to spectral steepenings, but which of them are realized or responsible for the observed spectrum is not clear at this point.
The effects are visible though, Zatsepin and Sokolskaya (2006) describe three classes of accelerators and differentiate them by their power-law index and cut-off energy. The first two classes have a power-law index of 2.3 and 2.1 and cut-off energies of 50 TeV and 4 PeV respectively. As the H.E.S.S. data only reaches up to 10 TeV, it does not suffice to conclude a cut-off of 50 TeV and 4 PeV in the proton spectrum, these cut-offs could be unveiled by measurements from future telescopes like HAWC and CTA. But, there seems to exist a class with indices between 2 and 2.3. Zatsepin and Sokolskaya (2006) conclude a best-fit power-law of 2.57 and a cut-off energy of 200 GeV for the third class, but attribute it to novae. Due to the small amount of flux needed in their model this might be a good conclusion, though the modeling of the supernova remnants in this work shows that supernova remnants exhibit such a spectral feature too, but with a far higher flux.
The available data about specific supernova remnants can be increased by more observations, especially at energies that are currently not available, e.g. from 100 keV–100 MeV which would be decisive in determining if the MeV–GeV radiation is of a hadronic source. Alternatively new telescopes like the CTA or HAWC (Dubus et al. 2012), which are in course of construction have a high probability of determining the amount of hadronically generated gamma radiation of certain remnants, as the electron spectra cut-off energy are at lower energies than their observation range. CTA will observe gamma radiation from about 10 GeV to more than 100 TeV, while HAWC will approximately cover the range of 500 GeV–50 TeV (Dubus et al. 2012).

3.3. Neutrinos Emission

Another appealing option are neutrino observations. The neutrino spectra generated by proton-proton interactions at supernova remnants were calculated in the framework of Kelner et al. (2006). The individual fluxes are depicted in Figure 11 for the respective supernova remnants.
The displayed neutrino fluxes include oscillations. The neutrino ratio of $(\nu_e : \nu_\mu : \nu_\tau) = (1 : 2 : 0)$ at the source due to $\pi^\pm$ decay becomes $(1 : 1 : 1)$, so that the total number of neutrinos of any kind

is 1/3 of the total number of neutrinos:

$$\Phi_{\nu_\mu+\bar{\nu}_\mu,\mathrm{osc}} \sim \frac{1}{3}\left(\Phi_{\nu_\mu} + \Phi_{\bar{\nu}_\mu} + \Phi_{\nu_\mathrm{e}} + \Phi_{\bar{\nu}_\mathrm{e}}\right). \quad (2)$$

Here, Φ is the neutrino flux of a certain species. Declination-averaged point source sensitivities of suitable neutrino observatories (ANTARES: Spurio (2009); IceCube: Kappes (2012); KM3NeT: Katz and Spiering (2012)) have been added to the plots. In the figures, we only roughly estimate the energy range of the limits from about 1 TeV up to 1 PeV as the approximate sensitivity range for point sources of detectors like IceCube, Antares and Km3NeT. The exact energy range depends on the concrete analysis. The current limits are given for a simple E^{-2} power law. In order to test the predicted fluxes concretely, they should be modeled with the predicted power-law behavior and an implemented cut-off, similar to what is already done for other sources by Abbasi et al. (2013).
In the northern hemisphere G40.5–0.5 seems to be a promising candidate that could be detected soon, previously already discussed by Halzen et al. (2008). IC443 could be of interest, unfortunately there is only on data point in the upper TeV domain so far (Abdo et al. 2009b). A larger amount of data would lead to a more precise estimate, with a possibly flatter spectrum. The current estimate can be seen as roughly at best.

4. Uncertainties

The results discussed here are based on a relatively small sample of supernova remnants. All statistical investigations like the correlation between the remnants age and $E_{\mathrm{max,e}}$ have to be confirmed by future measurements. It is expected that next generation telescopes like CTA and HAWC will both add a large number of sources and extended measurements systematically up to $> 10\,\mathrm{TeV}$. This gives a great opportunity to study the high-energy cut-off of the sources and helps to discriminate leptonic from hadronic sources.
The majority of supernova remnants is believed to be interacting with a molecular cloud. There are already some molecular clouds that are highly likely to be illuminated by cosmic rays (Aharonian et al. 2008d; Li and Chen 2012), which are searched for with interest. So there is a huge interest causing a large number of molecular cloud supernova remnants being observed. More than half of the selected supernova remnants are reported to be interacting with a molecular cloud, so the ratio of the first and second peak in Figure 8 is not statistically significant due to this possible selection effect.
In most cases using combined spectra of IC, bremsstrahlung, and π^0-decay with simple power-laws suffice to model the remnants, but usually broken power-laws have been employed to model the spectra of SNRs (e.g. Abdo et al. 2010c; Katagiri et al. 2011).
The tanh function in the assumed spectrum is in first order approximation a break in the power-law index by exactly one. This could mean the observed breaks in the electron spectrum by at least one are breaks instead of a minimum energy.
Furthermore, the electron spectra depend more strongly on the energy loss processes than the proton

spectra, which would mean that they possibly have a very different shape, e.g. the one suggested by Zirakashvili and Aharonian (2007). Applying this comes at the price of losing the comparability between the power-law indices of the electron and proton spectra, so it was not done in this work.

5. Conclusions

In this work various Galactic supernova remnants were modeled and analyzed for hadronic emission via π^0-decay as the majority of cosmic rays arriving at Earth are of hadronic nature. Here, we could show that a simple power-law with an upper cut-off energy typically suffices to model most remnants. Hadronic emission was found to be present at most Galactic supernova remnants, with a few exceptions. The distribution of the hadronic power-law indices allowed to group the remnants into two categories:

Class I A proton power-law index of $2.0 < \alpha_p < 2.3$. Which is from its current spectral energy distribution in the MeV–TeV domain indistinguishable from the shape of a bremsstrahlung dominated spectrum.

Class II A power-law index of $\alpha_p \gtrsim 2.6$. A sharp hadronic peak with a sudden decline exists in the MeV–GeV domain. The GeV–TeV domain is commonly dominated by bremsstrahlung or inverse Compton radiation in those cases.

However, a morphological or a progenitor-based origin was not examined in this work, although Class II seems to be common among the supernova remnants which interact with a molecular cloud in their vicinity.
The leptonic emission in the MeV–TeV range is found to often be dominated by bremsstrahlung instead of inverse Compton radiation for which models are prevalent in literature compared to bremsstrahlung-based emission models. The power-law indices of the electron spectrum scatter around the expected value of two.
An upper cut-off energy in the SNRs' electron spectrum that declines with the age of the object has been found by using all statistically determined cut-off energies of supernova remnants in the sample. This confirms the expectations based on the evolution of supernova remnants, and their declining shock speeds.

5.1. Outloook

The neutrino fluxes based on the hadronic part of the spectral energy distribution of the supernova remnants have been calculated and it was found that some of the Galactic supernova remnants can become visible soon by modern neutrino telescopes like IceCube and KM3NeT.
Still many results of this work have to be confirmed by higher statistics as only 24 of the 274

supernova remnants recorded within Green's Catalog (Green 2009) were used in this work. An improvement of the measured SED in particular concerning X-ray measurements to fix the electron cut-off would help to discriminate the different models even further.

The resulting proton and electron spectra from modeling the supernova remnants can be used for propagation, e.g. via GALPROP, to see if the cosmic ray spectrum at Earth is matched by the derived spectra. Furthermore the resulting neutrino spectra can be used as signal hypotheses for neutrino observatories.

Acknowledgements

MM thanks Miguel Araya-Arguedas, Evgeny Berezhko, and Takaaki Tanaka for the provision of data of unfolded X-Ray spectra for Cassiopeia A, SN 1006, and RX J1713.7–3946. MM also thanks Bon-Chul Koo, Dominik Bomans, and Marek Wezgowiec for the discussions and hints about synthesizing X-Ray spectra for this work. Discussions with P.L. Biermann & F. Schuppan are acknowledged by MM. JBT and MM acknowledge the support from the DFG in the framework of the research group FOR1048 on "Instabilities, turbulence and transport in cosmic magnetic fields" and from the Research Department of Plasmas with Complex Interactions (Bochum).

REFERENCES

Abbasi, R. et al. 2013, ApJ, 763, 33.

Abdo, A.A. et al. 2007, ApJ, 664, L91.

Abdo, A.A. et al. 2009a, ApJ, 706, L1.

Abdo, A.A. et al. 2009b, ApJ, 700, L127.

Abdo, A.A. et al. 2010a, ApJ, 710, L92.

Abdo, A.A. et al. 2010b, ApJ, 718, 348.

Abdo, A.A. et al. 2010c, Science, 327, 1103.

Abdo, A.A. et al. 2010d, ApJ, 712, 459.

Abdo, A.A. et al. 2010e, ApJ, 722, 1303.

Abdo, A.A. et al. 2011, ApJ, 734, 28.

Acciari, V.A. et al. 2009, ApJ, 698, L133.

Acciari, V.A. et al. 2010, ApJ, 714, 163.

Acciari, V.A. et al. 2011, ApJ, 730, L20.

Acero, F. et al. 2010, A&A, 516, A62.

Aharonian, F.A. and Atoyan, A.M. 1996, A&A, 309, 917.

Aharonian, F. et al. 2006, ApJ, 636, 777.

Aharonian, F. et al. 2007a, A&A, 464, 235.

Aharonian, F. et al. 2007b, ApJ, 661, 236.

Aharonian, F. et al. 2008a, A&A, 483, 509.

Aharonian, F. et al. 2008b, A&A, 490, 685.

Aharonian, F. et al. 2008c, A&A, 486, 829.

Aharonian, F. et al. 2008d, A&A, 481, 401.

Aharonian, F. et al. 2009a, A&A, 499, 723.

Aharonian, F. et al. 2009b, ApJ, 692, 1500.

Ajello, M. et al. 2012, ApJ, 744, 80.

Albert, J. et al, 2006a, ApJ, 637, L41.

Albert, J. et al. 2006b, ApJ, 643, L53.

Albert, J. et al. 2007a, A&A, 474, 937.

Albert, J. et al. 2007b, ApJ, 664, L87.

Aleksić, J. et al. 2012, A&A, 541, A13.

Allen, G.E. et al. 2001, ApJ, 558, 739.

Araya, M. and Cui, W. 2010, ApJ, 720, 20.

Baars, J.W.M. et al. 1977, A&A, 61, 99.

Bamba, A. et al. 2000, PASJ, 52, 259.

Bamba, A. et al. 2008, PASJ, 60, 153.

Beck, R. and Krause, M. 2005, Astronomische Nachrichten, 326, 414.

Becker, J.K. et al. 2011, ApJ, 739, L43.

Bell, A.R. 1978, MNRAS, 182, 147.

Blandford, R.D. and Ostriker, J.P. 1978, ApJ, 221, L29.

Blumenthal, G.R. and Gould, R.J. 1970, Rev. Mod. Phys., 42, 237.

Brogan, C.L. et al. 2005, ApJ, 629, L105.

Brogan, C.L. et al. 2006, ApJ, 639, L25.

Brun, F. et al. 2011, arXiv:1104.5003.

Cassam-Chenaï, G. et al. 2004, A&A, 427, 199.

Cassam-Chenaï, G. et al. 2007, ApJ, 665, 315.

Castelletti, G. et al. 2006, A&A, 459, 535.

Castelletti, G. et al. 2007, A&A, 471, 537.

Castro, D. and Slane, P. 2010, ApJ, 717, 372.

Caswell, J.L., Clark, D.H., and Crawford, D.F. 1975, Australian Journal of Physics Astrophysical Supplement, 37, 39.

Chen, Y. and Slane, P.O. 2001, ApJ, 563, 202.

Clauset, A. et al. 2009, SIAM Review, 51, 661.

Cox, D.P. 1972, ApJ, 178, 159.

Cox, D.P. et al. 1999, ApJ, 524, 179.

Dubus, G. et al. 2012, arXiv:1208.5686.

Duncan, A.R. and Green, D.A. 2000, A&A, 364, 732.

Erickson, W.C. and Mahoney, M.J. 1985, ApJ, 290, 596.

Galassi, M. et al. 2009, GNU Scientific Library Reference Manual (Network Theory).

Giordano, F. et al. 2012, ApJ, 744, L2.

Giuliani, A. et al. 2011, ApJ, 742, L30.

Goldsmith, P.F. and Mao, X.-J. 1983, ApJ, 265, 791.

Green, D.A. 2009, Bulletin of the Astronomical Society of India, 37, 45.

Halzen, F., Kappes, A., and Ó Murchadha, A. 2008, Phys. Rev. D, 78, 063004.

Harrus, I. et al. 2006, in The X-ray Universe 2005, Vol. 604 of ESA Special Publication, 369.

Hillas, A.M. 2005, J. of Phys. G: Nucl. Phys., 31, 95.

Hui, C.Y. et al. 2011, ApJ, 735, 115.

Hwang, U. and Laming, J.M. 2012, ApJ, 746, 130.

Inoue, T. et al. 2012, ApJ 744, 71.

Kappes, A. 2012, arXiv:1209.5855

Kassim, N.E. 1989, ApJS, 71, 799.

Kassim, N.E. and Weiler, K.W. 1990, ApJ, 360, 184.

Kassim, N.E., Weiler, K.W., and Baum, S.A. 1991, ApJ, 374, 212.

Katagiri, H. et al. 2011, ApJ, 741, 44.

Katz, U.F. and Spiering, C. 2012, Progress in Particle and Nuclear Physics, 67, 651.

Kelner, S.R., Aharonian, F.A., & Bugayov, V.V. 2006, Phys. Rev. D, 74, 034018

Koo, B.-C., Kim, K.-T., and Seward, F.D. 1995, ApJ, 447, 211.

Koo, B.-C., Lee, J.-J., and Seward, F.D. 2002, AJ, 123, 1629.

Lande, J. et al. 2012, ApJ, 756, 5.

LaRosa, T.N. et al. 2000, AJ, 119, 207.

Lazendic, J.S. et al. 2002, MNRAS, 331, 537.

Leahy, D.A. 2004, AJ, 127, 2277.

Leahy, D.A. and Tian, W.W. 2008, AJ, 135, 167.

Li, H. and Chen, Y. 2012, MNRAS, 421, 935.

Lemoine-Goumard, M. et al. 2012, A&A, 545, A28.

Malkov, M.A., Diamond, P.H., and Sagdeev, R.Z. 2012, Physics of Plasmas, 19, 082901.

Morlino, G. and Caprioli, D. 2012, A&A, 538, A81.

Nakamura, R. et al. 2009, PASJ, 61, 197.

Nelder, G.R. and Mead, R.J. 1965, The Computer Journal, 7, 308.

Nolan, P.L. et al. 2012, ApJS, 199, 31.

Padovani, M. et al. 2009, A&A, 501, 619.

Petre, R. et al. 1982, ApJ, 258, 22.

Petre, R., Becker, C. M., and Winkler, P.F. 1996, ApJ, 465, L43.

Reynolds, S.P. and Ellison, D.C. 1992, ApJ, 399, L75.

Roger, R.S. et al. 1986, MNRAS, 219, 815.

Schlickeiser, R. 2002, Cosmic Ray Astrophysics (Springer).

Schuppan, F. et al. 2012, A&A, 541, A126.

Sezer, A. et al. 2011, MNRAS, 417, 1387.

Slane, P. et al. 2012, ApJ, 749, 131.

Spurio, M. 2009, International Journal of Modern Physics D, 18, 1615.

Strong, A.W., Moskalenko, I.V., and Ptuskin, V.S. 2007, Annual Review of Nuclear and Particle Science, 57, 285.

Tanaka, T. et al. 2008, ApJ, 685, 988.

Tanaka, T. et al. 2011, ApJ, 740, L51.

Tavani, M. et al. 2010, ApJ, 710, L151.

Tian, W.W. and Leahy, D.A. 2012, MNRAS, 421, 2593.

Uchiyama, Y. et al. 2012, ApJ, 749, L35.

Uyanıker, B. et al. 2004, A&A, 426, 909.

Velázquez, P.F. et al. 2002, AJ, 124, 2145.

Williams, B.J. et al. 2011, ApJ, 741, 96.

Yang, J. et al. 2006, Chinese J. Astron. Astrophys., 6, 210.

Zatsepin, V.I. and Sokolskaya, N.V. 2006, A&A, 458, 1.

Zirakashvili, V.N. and Aharonian, F. 2007, A&A, 465, 695.

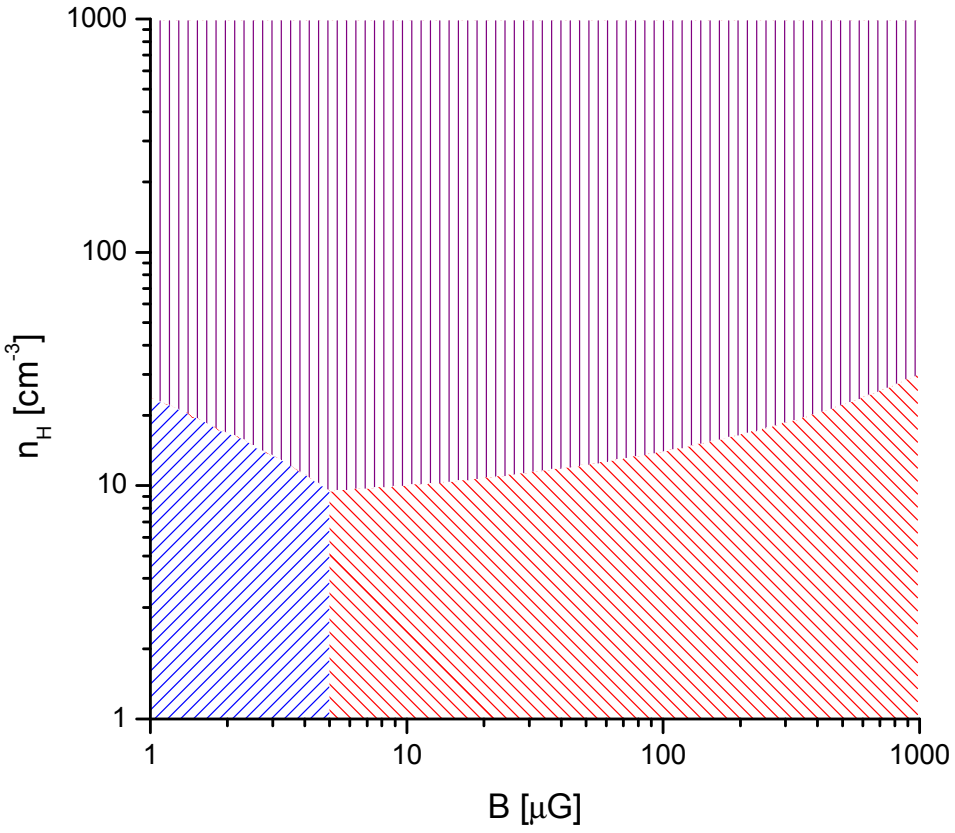

Fig. 1.— Dominant emission at 100 GeV depending on ambient proton density and magnetic field strength. The sychrotron emission has been kept constant and the total number of accelerated protons and electrons equal. The power-law indices of electron and proton spectrum are 2.0. Bremsstrahlung dominates the emission in the vertically slashed area, π^0-decay in the backslashed area, and IC scattering in the slashed area.

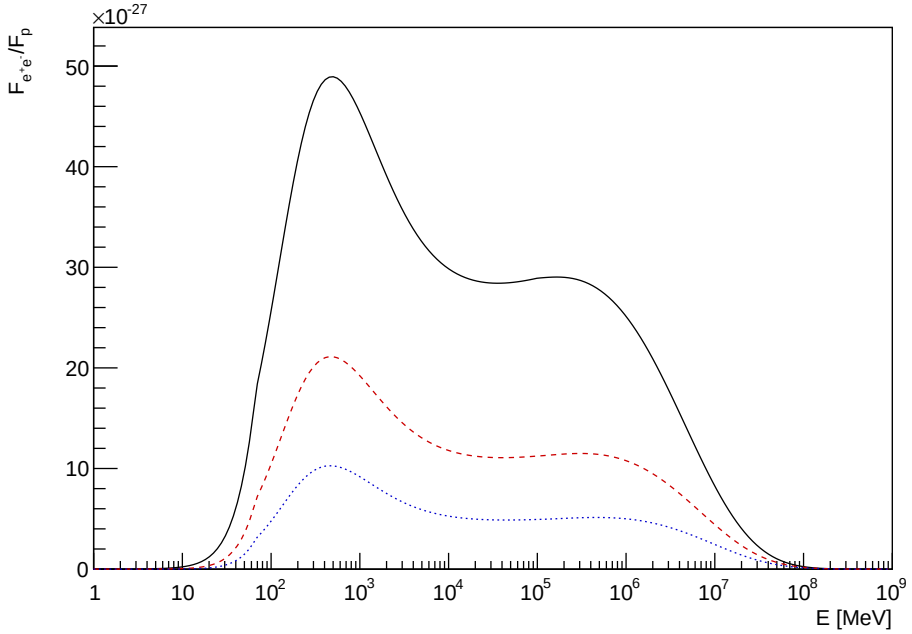

Fig. 2.— Flux ratio of secondary electrons and positrons to primary protons for power-law indices of 2.0 (solid), 2.3 (dashed), 2.6 (dotted).

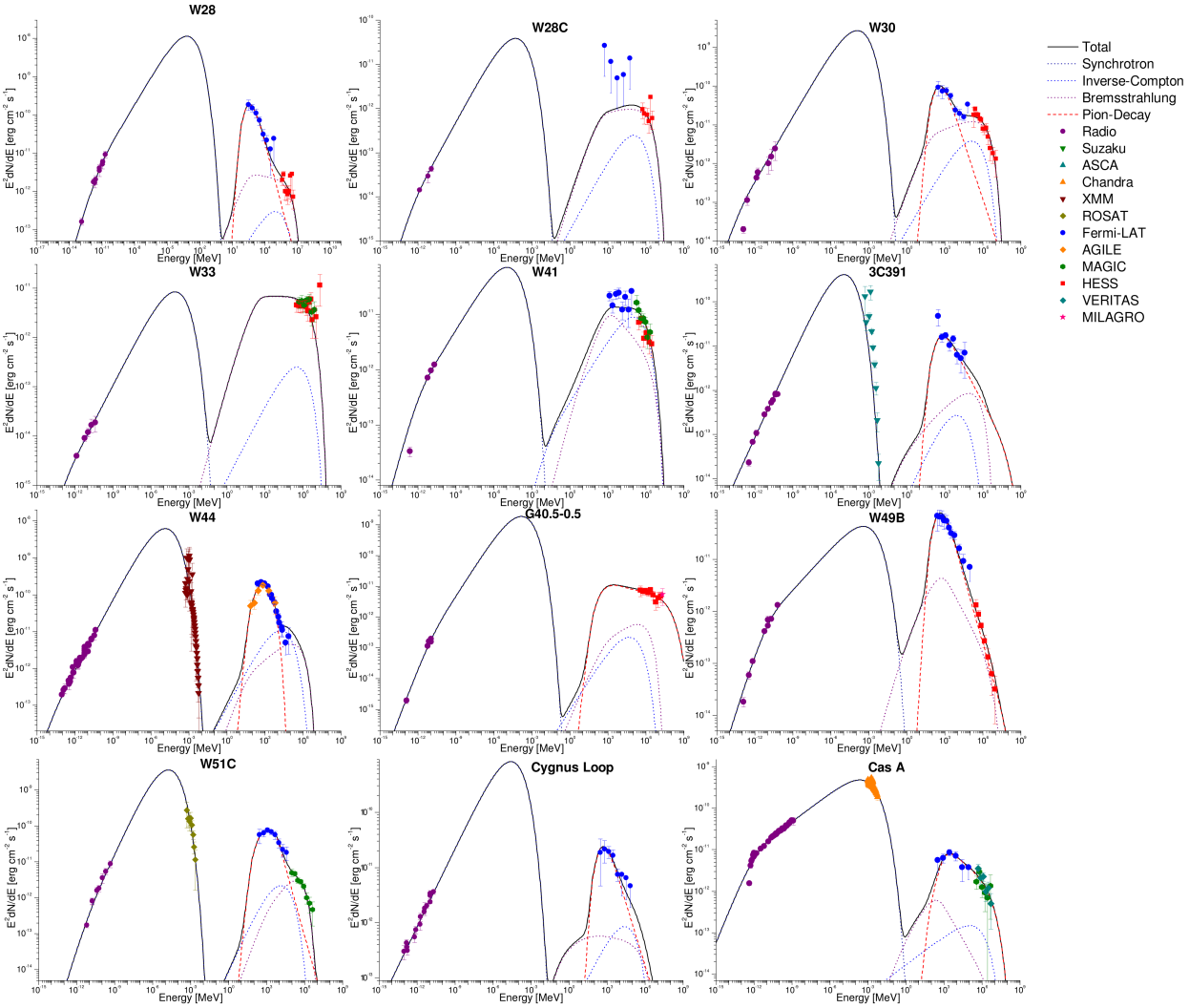

Fig. 3.— Modeled SEDs of the first twelve SNRs.

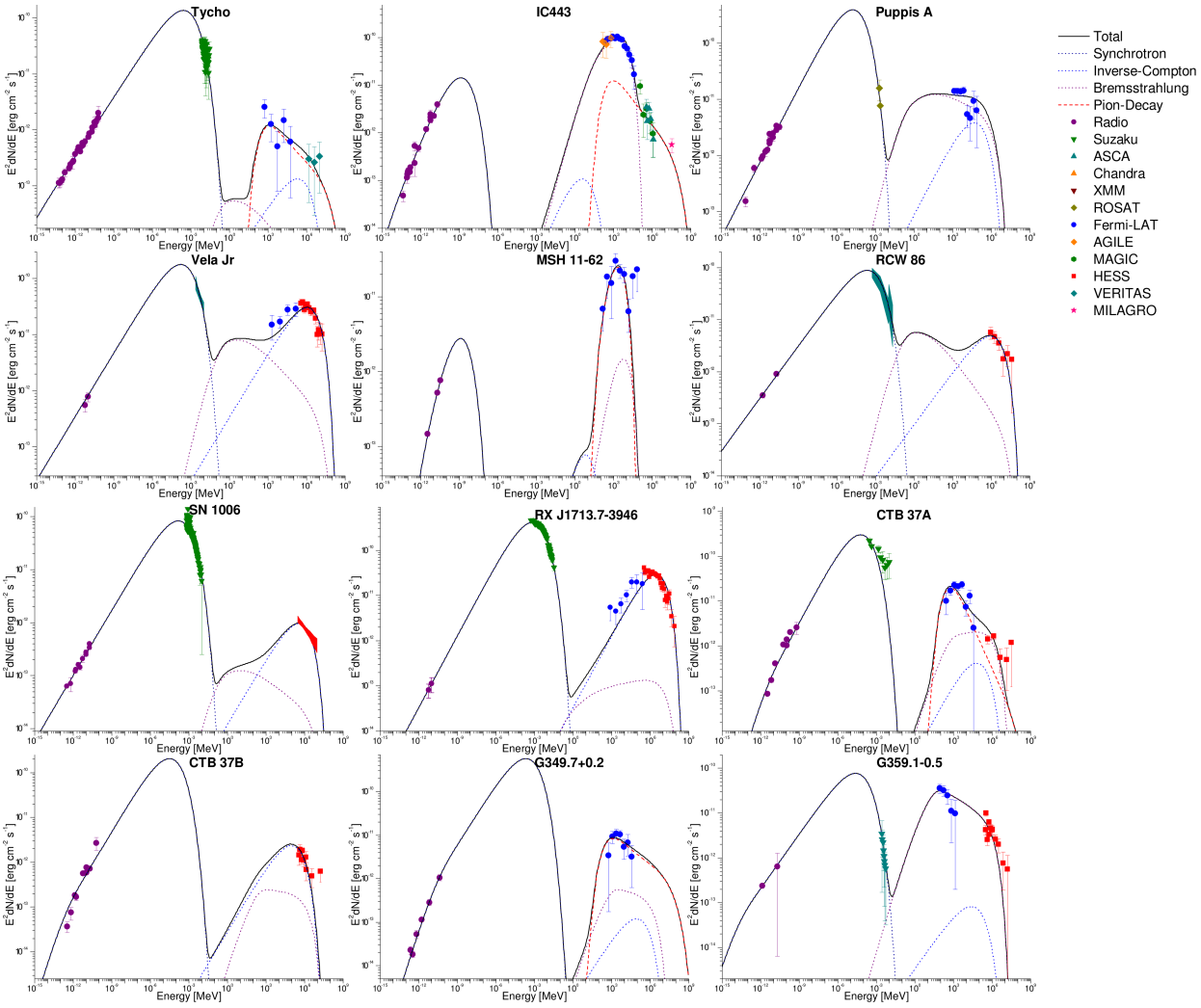

Fig. 4.— Modeled SEDs of the last twelve SNRs.

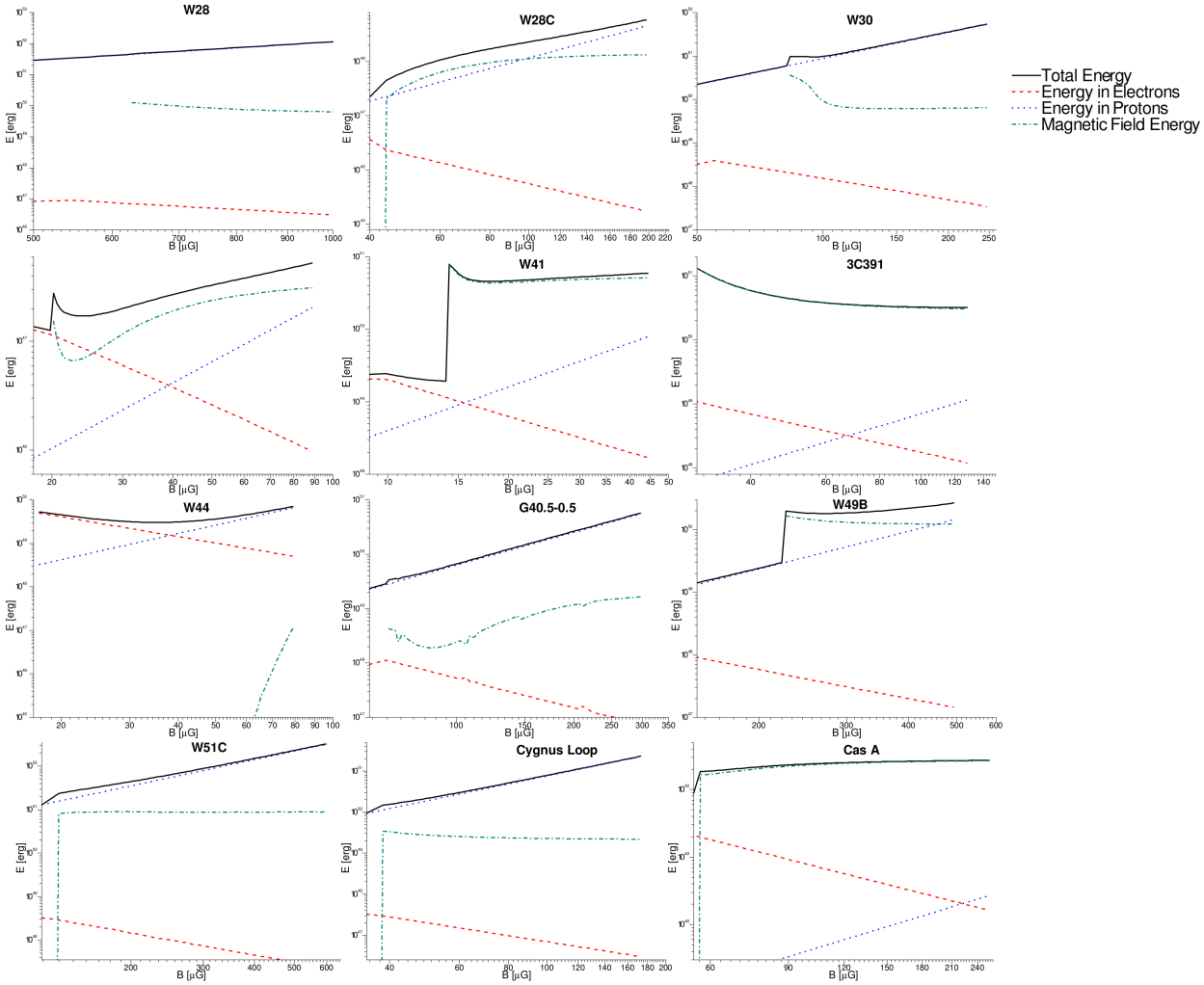

Fig. 5.— Energy in electrons, magnetic field, and protons versus magnetic field strength for the first twelve SNRs.

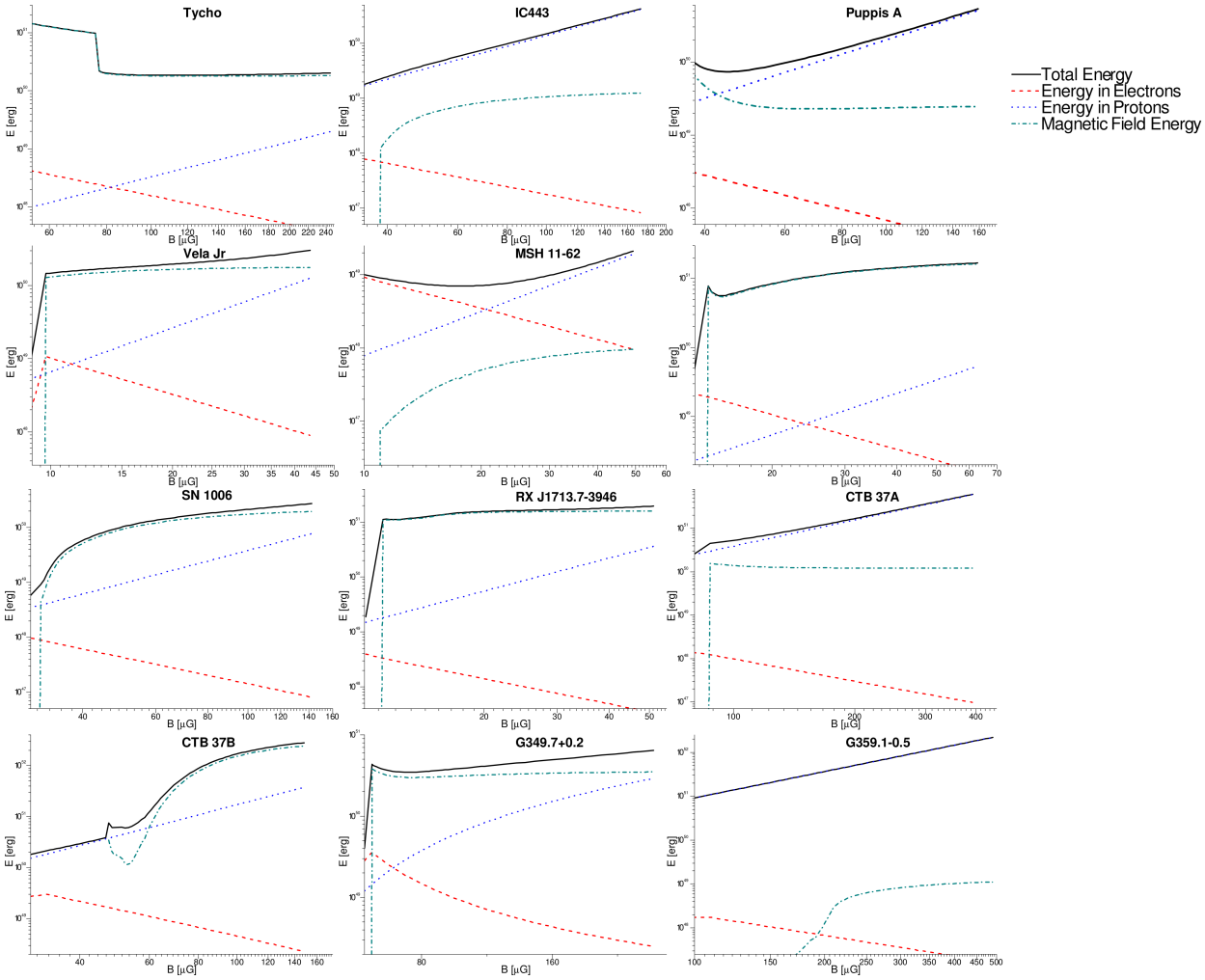

Fig. 6.— Energy in electrons, magnetic field, and protons versus magnetic field strength for the last twelve SNRs.

Table 1: Overview of the supernova remnants studied in this work. The columns of MeV–GeV and GeV–TeV indicated by which process the radiation is dominated in that range assuming the scenario of minimum energy: **B**remsstrahlung, inverse **C**ompton radiation, or **P**ion decay. A hadronical scenario, if possible is indicated in parentheses. The energy column indicates the source of energy that dominates the remnant: **E**lectrons, **M**agnetic field, or **P**rotons. The + in the age column indicates more than one order of magnitude uncertainty up from the presented minimal value, all other ages are averages of the suggested value range.

SNR	Dist. [kpc]	Age [yr]	$B_{\rm min}$ [μG]	$B_{\rm eq}$ [μG]	MeV–GeV	GeV–TeV	Energy
W28	1.9	33000+	500	620	P	B(P)	M
W28C	1.9	?	40	40	B(P)	B(P)	M/P
W30	4	25000	100	110	P	B+C	M
W33	4	1200	18	18	B?(P)	B(P)	P
W41	4.2	100000	9	9	B(P)	B(P)	P
3C391	7.2	4000	27	130	P	P	P
W44	3	10000	40	130	P	B	M
G40.5–0.5	3.4	30000	90	159	P	P	M
W49B	10	1000+	100	307	P	P	P
W51C	7.2	26000	120	130	P	B	M
Cygnus Loop	0.58	14000	35	100	P	P	M
Cassiopeia A	3.5	332	37	?	B(P)	C(P)	P
Tycho	3.5	440	45	100	P	P	P
IC443	1.5	3000+	35	40	B	B+P	M
Puppis A	2	4500	33	33	B(P)	B+C(P)	M/P
Vela Jr	1.3	2500	9	9	C(P)	C(P)	P
MSH 11–62	6.2	1300+	10	21	P	–	E+M
RCW 86	2.3	1827	13	13	?	C	P
SN 1006	2.2	1006	29	30	?(P)	C(P)	P
RX J1713.7	3.5	1619?	27	10	C	C	P
CTB 37A	7.9	2000	138	?	P	P/B?	M
CTB 37B	13.2	1750	30	30	C(P)	C(P)	P
G349.7+0.2	18.3	3500	45	>100	P	P	P
G359.1–0.5	7.6	10000+	41	41	B	B	M

Table 2: Second overview table of the supernova remnants studied in this work. A hadronical scenario, if possible is indicated in parentheses.

SNR	$n_{\rm H}$ [cm^{-3}]	$\alpha_{\rm e}$	$\alpha_{\rm p}$	$E_{\rm tot,e}$ [10^{47} ergs]	$E_{\rm tot,p}$ [10^{47} ergs]	Refs
W28	140	2.04	3.12(2.85)	0.70(0.26)	$1.2 \times 10^3 (6.0 \times 10^2)$	[1–4]
W28C	100	1.95	?(2.30)	0.36(0.11)	?(7.7)	[1,3–5]
W30	100	1.89	2.88	15	2.3×10^3	[6–9]
W33	1000	2.01	?(1.80)	1.3(0.1)	?(3.1)	[9–12]
W41	6	2.25	?(2.30)	206(17)	$?(5.3 \times 10^3)$	[2,9,13–15]
3C391	15	1.75	2.60	12	3.1×10^3	[2,7,16]
W44	6	1.80	2.59	25	183	[17–22]
G40.5–0.5	60	1.62	2.06	2.3	161	[2,23-25]
W49B	100	2.47	2.92	3.0	1.3×10^3	[2,26,27]
W51C	10	1.44	2.36 | 3.32	29	7.9×10^3	[28–31]
Cyg. Loop	5	2.05	2.81	0.67	227	[32,33]
Cas A	1.85	2.50	2.06(2.25)	218(29)	$2.2 \times 10^3 (3.9 \times 10^3)$	[34–39]
Tycho	0.65	2.29	2.31	16	1.8×10^3	[40–43]
IC443	100	1.70	2.22	8.4	3.0	[44–50]
Puppis A	20	2.11	?(2.41)	43(5)	?(243)	[51–54]
Vela Jr	1.55	2.14	?(1.84)	60(23)	$?(1.8 \times 10^3)$	[55–57]
MSH 11–62	7	1.23	1.68	31	5.5	[58,59]
RCW 86	2	2.33	?	220	?	[60–61]
SN 1006	1	2.18	?(2.35)	10(1.6)	$?(1.7 \times 10^3)$	[64–66]
RX J1713.7	0.65	1.94	?	39	?	[67–71]
CTB 37A	100	2.00	?	4.8	610	[7,72–75]
CTB 37B	1.6	2.04	?(2.52)	275(45)	$?(1.6 \times 10^5)$	[74,76,77]
G349.7+0.2	65	2.07	2.30	25	3.6×10^3	[2,7]
G359.1–0.5	10000	2.21	?	23	?	[9,78–81]

References. [1] Velázquez et al. (2002); [2] Kassim (1989); [3] Abdo et al. (2010b); [4] Aharonian et al. (2008d); [5] Brogan et al. (2006); [6] Kassim and Weiler (1990); [7] Castro and Slane (2010); [8] Ajello et al. (2012); [9] Aharonian et al. (2006); [10] Goldsmith and Mao (1983); [11] Brogan et al. (2005); [12] Albert et al. (2006a); [13] Leahy and Tian (2008); [14] Li and Chen (2012); [15] Albert et al. (2006b); [16] Chen and Slane (2001); [17] Cox et al. (1999); [18] Castelletti et al. (2007); [19] Harrus et al. (2006); [20] Giuliani et al. (2011); [21] Abdo et al. (2010c); [22] Uchiyama et al. (2012); [23] Yang et al. (2006); [24] Aharonian et al. (2009a); [25] Abdo et al. (2007); [26] Abdo et al. (2010e); [27] Brun et al. (2011); [28] Koo et al. (1995); [29] Koo et al. (2002); [30] Abdo et al. (2009a); [31] Aleksić et al. (2012); [32] Katagiri et al. (2011); [33] Uyanıker et al. (2004); [34] Hwang and Laming (2012); [35] Baars et al. (1977); [36] Araya and Cui (2010); [37] Abdo et al. (2010a); [38] Albert et al. (2007a); [39] Acciari et al. (2010); [40] Cassam-Chenaï et al. (2007); [41] Reynolds and Ellison (1992); [42] Giordano et al. (2012); [43] Acciari et al. (2011); [44] Leahy (2004); [45] Erickson and Mahoney (1985); [46] Tavani et al. (2010); [47] Abdo et al. (2010d); [48] Albert et al. (2007b); [49] Abdo et al. (2009b); [50] Acciari et al. (2009); [51] Petre et al. (1982); [52] Petre et al. (1996); [53] Castelletti et al. (2006); [54] Lande et al. (2012); [55] Duncan and Green (2000); [56] Tanaka et al. (2011); [57] Aharonian et al. (2007b); [58] Roger et al. (1986); [59] Slane et al. (2012); [60] Williams et al. (2011); [61] Caswell et al. (1975); [62] Lemoine-Goumard et al. (2012); [63] Aharonian et al. (2009b); [64] Allen et al. (2001); [65] Bamba et al. (2008); [66] Acero et al. (2010); [67] Cassam-Chenaï et al. (2004); [68] Abdo et al. (2011); [69] Lazendic et al. (2002); [70] Tanaka et al. (2008); [71] Aharonian et al. (2007a); [72] Tian and Leahy (2012); [73] Sezer et al. (2011); [74] Kassim et al. (1991); [75] Aharonian et al. (2008b); [76] Nakamura et al. (2009); [77] Aharonian et al. (2008c); [78] LaRosa et al. (2000); [79] Bamba et al. (2000); [80] Hui et al. (2011); [81] Aharonian et al. (2008a).

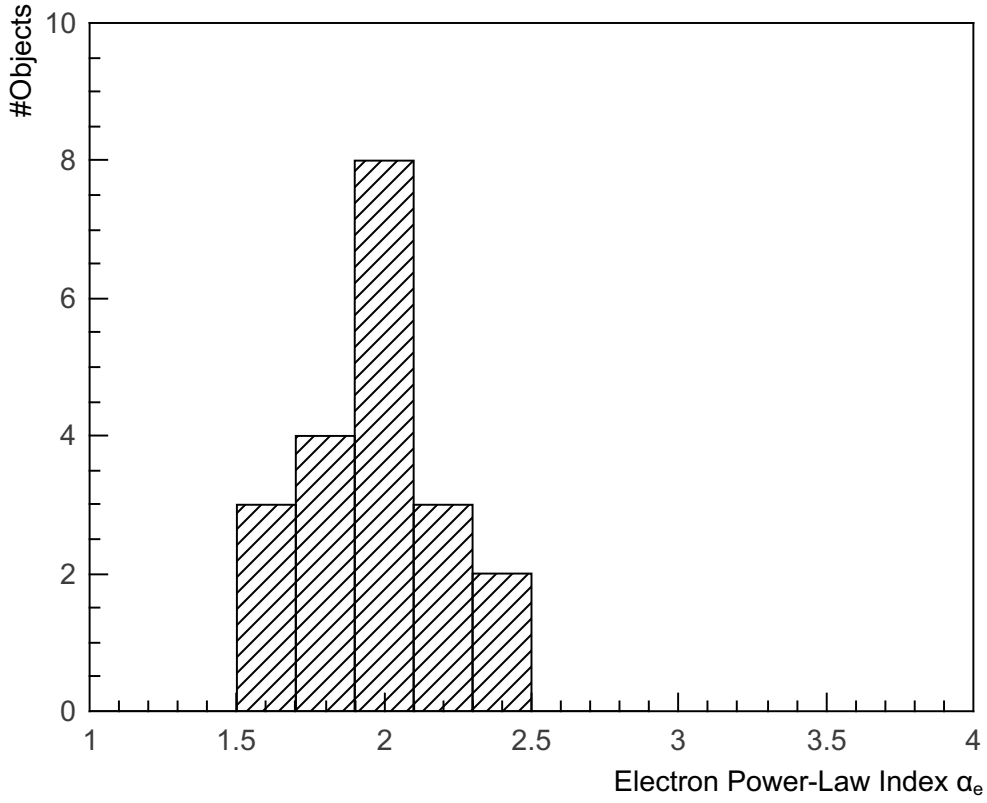

Fig. 7.— Number of occurrences of the spectral indices of the electron spectrum for the modeled supernova remnants. Spectral indices with an error larger than the bin size 0.2 were not included.

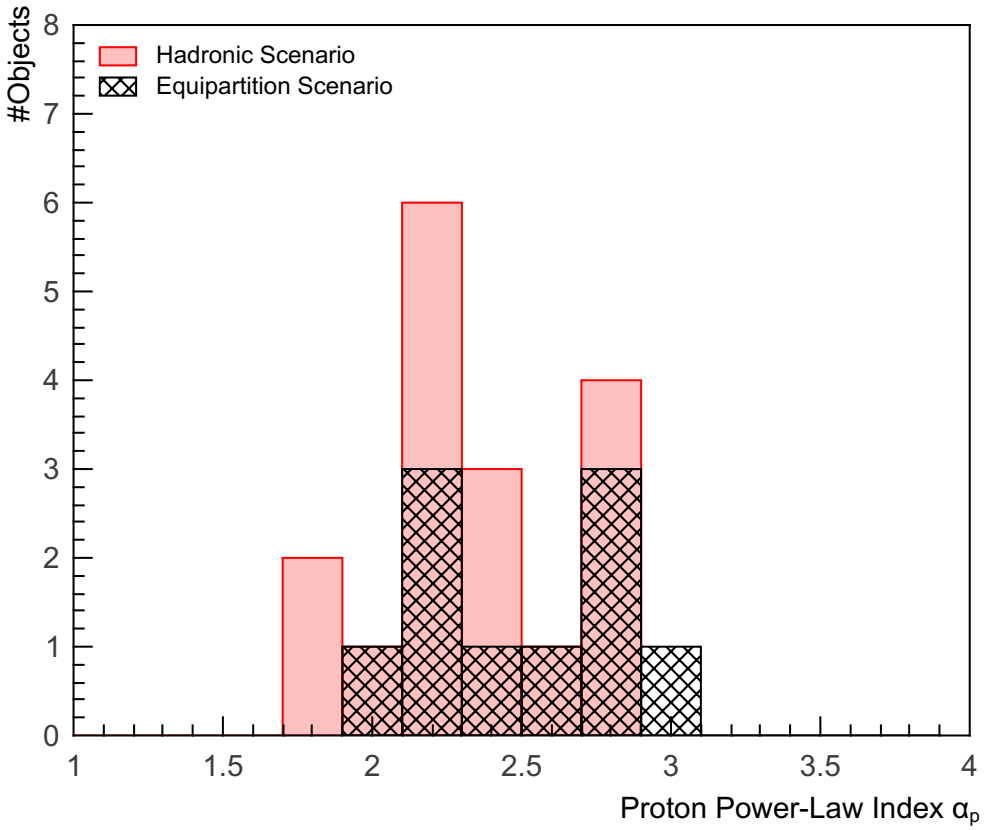

Fig. 8.— Number of occurrences of the spectral indices of the proton spectrum for the modeled supernova remnants. All possible remnants were taken into account. Spectral indices with an error larger than the bin size 0.2 were not included. The two distributions distinguish between the minimizing energy scenario (grid patterned bars) and the hadronic scenario (grey shaded bars).

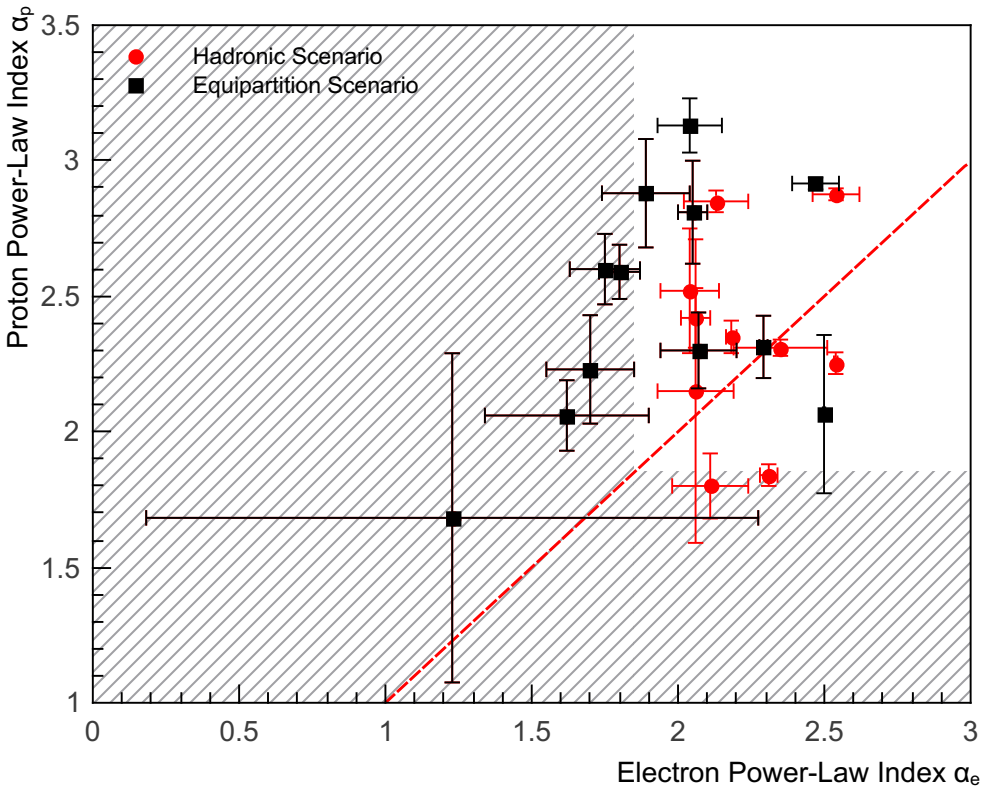

Fig. 9.— Spectral index of the proton spectrum versus spectral index of the electron spectrum of SNRs which are likely to be in a hybrid or hadronic state. The dashed line represents the case of equal spectral indices ($\alpha_e = \alpha_p$). The crossed out areas represent unphysical conditions with too flat primary spectra.

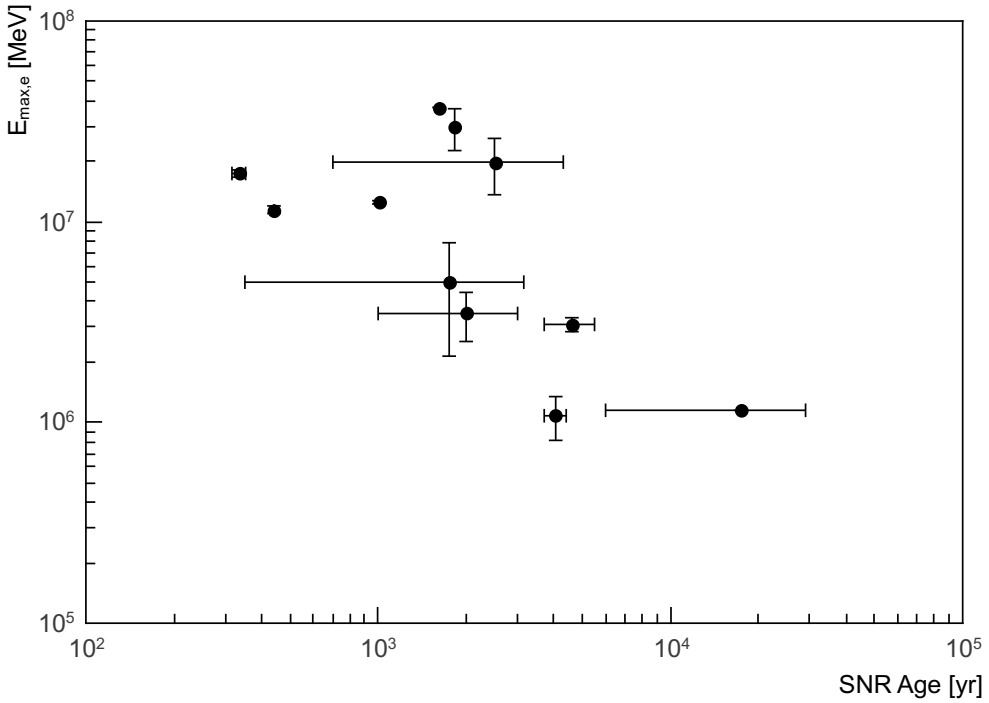

Fig. 10.— Cut-off energies of the electron spectrum versus the age of the remnant. Only remnants with cut-offs implied by X-Ray observations have been used.

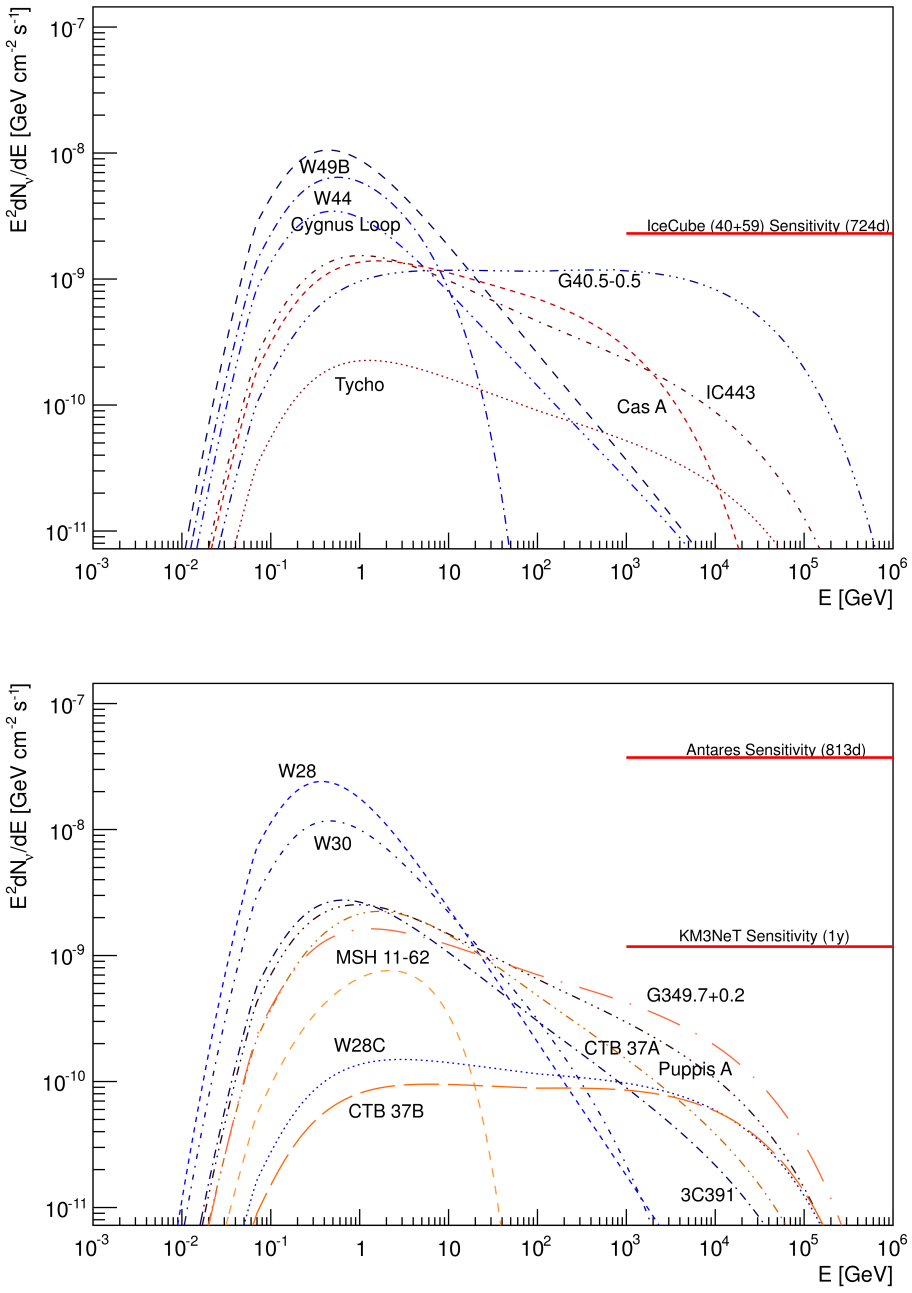

Fig. 11.— Predicted neutrino fluxes from the modeled supernova remnants in the northern hemisphere (upper) and southern hemisphere (lower). All possible hadronic fluxes have been selected for this graph. Flux density limits for an average declination angle of the IceCube Neutrino Observatory (Kappes 2012), ANTARES (Spurio 2009) and KM3NeT (Katz and Spiering 2012) have been added.